Nuclear Engineering and Technology 50 (2018) 145–150

Contents lists available at ScienceDirect

Nuclear Engineering and Technology

journal homepage: www.elsevier.com/locate/net

Original Article

A new gas–solid reaction model for voloxidation process with spallation

Je Ir Ryu [a], Seung Min Woo [b, *]

[a] Department of Mechanical Engineering, University of California – Berkeley, Berkeley, CA 94720, USA
[b] Department of Nuclear Engineering, University of California – Berkeley, Berkeley, CA 94720, USA

ARTICLE INFO

Article history:
Received 30 August 2017
Received in revised form
9 November 2017
Accepted 15 November 2017
Available online 9 December 2017

Keywords:
Crack–Spallation Model
Gas–Solid Reactions
Shrinking Core Model
Voloxidation

ABSTRACT

A new methodology, the crack–spallation model, has been developed to analyze gas–solid reactions dominated by crack growth inside of the solid reactant and spallation phenomena. The new model physically represents three processes of the reaction progress: (1) diffusion of gas reactant through pores; (2) growth of product particle in pores; and (3) crack and spallation of solid reactant. The validation of this method has been conducted by comparison of results obtained in an experiment for oxidation of UO_2 and the shrinking core model. The reaction progress evaluated by the crack–spallation model shows better agreement with the experimental data than that evaluated by the shrinking core model. To understand the trigger point during the reaction progress, a detailed analysis has been conducted. A parametric study also has been performed to determine mass diffusivities of the gas reactant and volume increase constants of the product particles. This method can be appropriately applied to the gas–solid reaction based on the crack and spallation phenomena such as the voloxidation process.

1. Introduction

One well-known methodology to analyze gas–solid reactions is the shrinking core model (SCM) [1]. An approximated solution of this model is widely explained in standard textbooks [2,3], as follows. In the SCM, the gas reacts with the reactant material at the surface, and the reaction zone moves inward of the reactant, as shown in Fig. 1. In other words, the unreacted solid sequentially shrinks. The completely reacted solid remains at its original locations, and is called "ash." It is assumed that (1) all particles are identical and do not vary during the reaction and (2) the densities of particles and solid reactant are similar. Then, for a simple gas–solid reaction defined as

$$A(gas) + bB(solid) \rightarrow cC(solid), \tag{1}$$

where A is the gas reactant, B is the solid reactant, C is the solid product, and b and c are stoichiometric coefficients, the governing equation for the one-dimensional diffusion of the gas reactant into the solid reactant is

$$\frac{\partial C_A}{\partial t} = D_e\left(\frac{\partial^2 C_A}{\partial r^2} + \frac{N}{r}\frac{\partial C_A}{\partial r}\right), \tag{2}$$

where C_A is the molar concentration of A, t is the time, D_e is the effective mass diffusivity, N is the geometry factor ($N = 0$, rectangular coordinate; $N = 1$, cylindrical coordinate; and $N = 2$, spherical coordinate), and r is the spatial coordinate (r should be replaced by x for the rectangular coordinate). The governing equation can be solved by applying the quasi-steady-state approximation. To show how much the reactant material has been reacted, a parameter, X_B, is defined as

$$X_B(t) = 1 - \left(\frac{R(t)}{R_0}\right)^{N+1}, \tag{3}$$

where R is the radius of unreacted solid material and R_0 is the initial radius of the solid reactant. With appropriate boundary and initial conditions for a cylindrical solid reactant, the analytical solution can be derived as

* *Corresponding author.*
E-mail address: woosm@berkeley.edu (S.M. Woo).

https://doi.org/10.1016/j.net.2017.11.005

$$t = \frac{\rho_{Bm} R_0}{b C_{Ag}} \left[\frac{1}{2k_{Ag}} X_B + \frac{R_0}{4D_e} \{X_B + (1 - X_B)\ln(1 - X_B)\} + \frac{1}{k_{As}} \left\{ 1 - (1 - X_B)^{1/2} \right\} \right], \quad (4)$$

where ρ_{Bm} is the molar density of the solid reactant, C_{Ag} is the molar concentration of the gas reactant in the bulk gas, k_{Ag} is the mass transfer coefficient of the gas reactant between the gas film and the ash layer, and k_{As} is the rate constant for a first-order surface reaction at the solid reactant surface.

Many researchers have attempted further expansion and modification of the SCM. The Johnson–Mehl equation has been applied to the chemical reaction resistance term in Eq. (4) [4]. The particle size distribution of the solid material has been coupled with the SCM [5]. The varying of the ash zone size during the reaction time has been mathematically applied by modifying the SCM [6]. Shi et al. [7] modified the SCM to study methane hydrates in a dry-water droplet. Comparisons of the SCM applying the assumption of quasi-static diffusion against without that also have been conducted [8]. These SCM-based methods basically assume that chemical reaction and loss of solid reactant occur on the solid surface.

However, according to experimental studies, for example, considering the oxidation behavior of UO_2 pellets [9], a gas–solid reaction can progress mainly by cracks growing and spallation of a solid reactant because of volume changes from the transformation of reactants into product in pores and grain boundaries of the solid reactant. Therefore, the SCM method, based on the demonstration of a gas film within the bulk gas, the diffusion of the gas through the ash layer, and shrinking of the reactant material by the surface chemical reaction, cannot physically describe the crack and spallation mechanism for this type of gas–solid reaction. In this study, a new kinetic model for gas–solid reactions has been proposed to demonstrate reactions dominated by crack and spallation rather than surface chemistry.

2. Kinetic model

2.1. Crack–spallation model

To begin with, let us consider a simple gas–solid reaction as described in Eq. (1). If the reaction progress is dominated by cracks and spallation from the growth of the product particle in the pores, the reaction process can be illustrated as shown in Fig. 2. In this model, we assume that (1) the spherical pores are uniformly distributed in the media with identical physical features, for example, the physical shape and size; (2) cracks and spallation occur at pore locations when the product particle size is larger than the pores; (3) pores have enough space to generate and grow particles; (4) product particles are spherical and grow one-dimensionally; (5) the reaction progress by surface chemistry is much slower than that by cracks and spallation; (6) the chemical reaction time for spalled solid reactants is not considered, because it could be negligible compared with the whole reaction progress time due to dramatic increase of the surface area; (7) the diffusion process is one-dimensional; (8) the diffusivity is constant in the solid reactant during the entire reacting time; (9) there is a sufficient amount of gas reactant around the solid reactant; and (10) the spalled reactant does not affect the diffusion of the gas reactant into the solid reactant.

There are three main processes for this model. The first process is the diffusion of gas reactant through pores, which are assumed to include all kinds of porous spaces such as cracks, fractures, grain boundaries, and porous vacancies in the solid reactant. Then, the diffused gas in the solid reactant starts to react with the solid reactant, as shown in Fig. 2b. This is the second process, which is the growth of product particles in pores. Because the amount of solid reactant is sufficient to react with the gas reactant, the dominant factor for the control of the gas–solid reaction in the pores is the concentration of diffused gas reactant in those pores. Finally, as illustrated in Fig. 2d, when the size of the product particles becomes greater than the size of the pores, the part of the solid reactant including that pores starts to crack and spall out.

2.2. Computation methodology

First, the diffusion process is solved by numerical calculation of the diffusion equation shown in Eq. (2). At the beginning of this process, there are no products, C (solid), inside of the solid reactant because of the lack of diffusing gases at this point. This initial condition is represented as

$$C_A(r < R_0, t = 0) = 0. \quad (5)$$

The boundary condition shown in Eq. (6) is that the molar concentration of gas reactant, C_A, at the surface of the solid reactant at a certain time, t, is equal to that in the air, C_{Ag};

$$C_A(r = R, t) = C_{Ag}. \quad (6)$$

The growth process is governed by the concentration of gas reactant in the pores, as explained in the previous section. After the diffusing of the gas reactant into the solid reactant, the generation of solid product particles begins. The produced solid particles inside the pores sequentially grow by continuous gas–solid chemical reaction. For this growth model, it is assumed that the volumetric growth rate of the product is modeled as a linear function of the gas concentration in the pores:

$$\frac{dV}{dt} = kC_A, \quad (7)$$

where V is the volume of the product in each pore and k is a constant. Then, the equation can be rewritten as

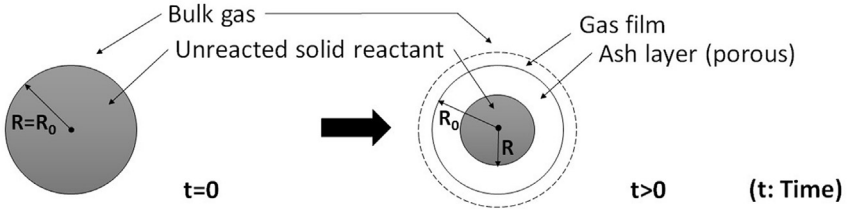

Fig. 1. Configuration of the SCM for an isothermal spherical reactant [3].

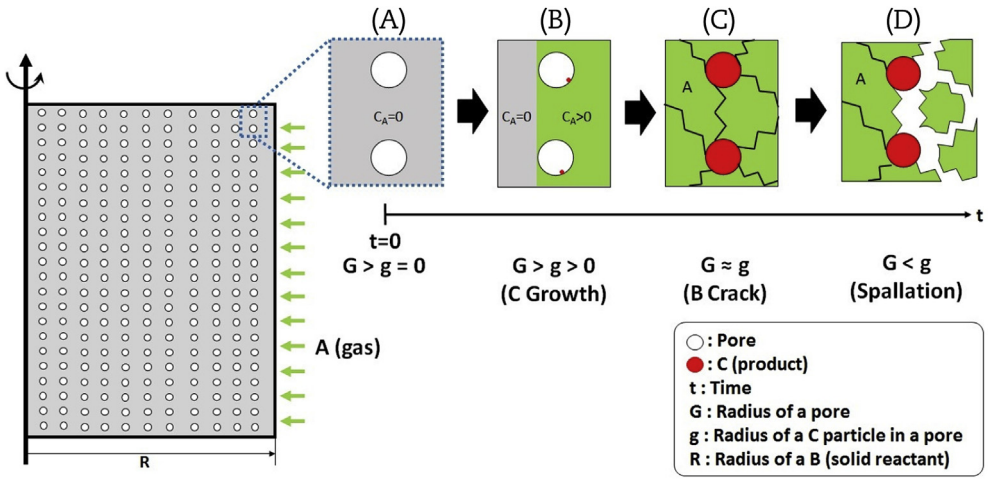

Fig. 2. Schematic layout of the crack–spallation model for gas–solid reactions.

$$\frac{dg}{dt} = \frac{3}{4\pi} k C_A \frac{1}{g^2}, \tag{8}$$

where g is the radius of the product particles in each pore. Even though C_A changes over time, it can be assumed to be a constant during a single numerical time step for the particle growth calculation because the gas diffuses into the porous media and this diffusion reaches equilibrium state in a very short time compared with the particle growth time. Based on this, the analytical solution to Eq. (8) is

$$g_{i+1} = 3^{1/3}\left[\frac{3}{4\pi} k C_{A,i} \Delta t + \frac{g_i^3}{3}\right]^{1/3}, \tag{9}$$

where the subscript i represents the value of the i^{th} time step and Δt is the time interval. These diffusion and growth equations are solved sequentially the each time step.

Finally, a part of the solid reactant can spall out at the moment that the size of the grown product particles, g, is greater than the size of the pores, G. As the pores are uniformly distributed and the gas reactant diffuses from the outside in a radial direction, the solid product particles in the pores located at the same column line grow identically. Therefore, the spallation progression proceeds only in the horizontal axis direction. The rest of the solid reactant in the spalled part can quickly react with the gas reactant because the reaction surface area is dramatically increased and the fragments are exposed to an environment in which the concentration of gas reactant is sufficiently high for active reactions. As a result, the chemical reaction time for the spalled parts has not been taken into account in the current model. Once spallation is found to have occurred, the volume of the solid reactant becomes smaller. The updated radius of the unreacted solid material, R, and the boundary condition for the diffusion equation are applied. Then, the diffusion and particle growth equations are repeatedly computed. The overall mechanism is described in the flow chart shown in Fig. 3.

2.3. Validation of the crack–spallation model

To validate the crack–spallation model, experimental data for the oxidation of uranium dioxide (UO_2) have been used. The overall reaction is

$$3UO_2(s) + O_2(g) \rightarrow U_3O_8(s). \tag{10}$$

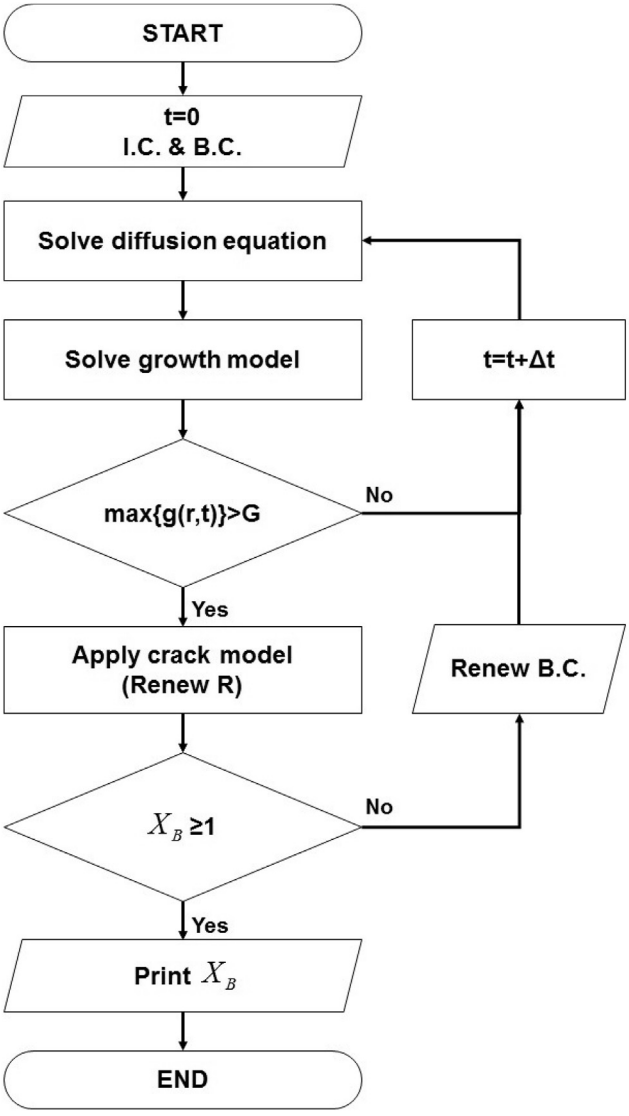

Fig. 3. Flowchart of numerical analysis for the crack–spallation model.

This reaction is applied in the voloxidation process. This process is one of the processes in the pyroprocessing system, which is used to recover useful actinides in spent nuclear fuels [10]. It was originally developed by Oak Ridge National Laboratory [11], and has been adopted as one of the head-end processes by the Korea Atomic Energy Research Institute [12]. Changing of a cylindrical UO_2 pellet to powder type (U_3O_8) in the voloxidation process enhances the performance of the electrolytic-reduction process by increasing the surface area [13]. Moreover, because there are volatile fission products (i.e., iodine, carbon, xenon, krypton, etc.) in spent fuel, those are removed and separated from the spent fuel during the voloxidation process [14,15]. Criticality [16] and shielding analysis [17] of the voloxidation process have been conducted. To analyze the performance of the process, Jeong et al. [4] and Park and Seo [13] adapted the SCM combined with the Johnson-Mehl equation. However, according to previous studies [9,18], the voloxidation process is dominated by crack and spallation. This is why it was selected for validation of the crack–spallation model.

The necessary input parameters and additional assumptions for the numerical simulation are as follows. O_2 is the gas reactant (A), and UO_2 is used as a solid reactant (B) in a pellet type. U_3O_8 is the product particle (C) in the pores. The size of the pores is determined based on the previous study [19], in which the mean diameter and the number density of the fission gas bubbles were analyzed with respect to burnup. As a reference case, we select the discharged burnup condition of 44 MWd/kgU, which is the typical burnup level. For that burnup case, the mean diameter and the number density of fission gas bubbles are 516 nm and 1.0×10^{18} #/m^3, respectively. The diameter of the nuclear fuel pellet is 0.71 cm [20]. The molar concentration of O_2 in air is evaluated based on the ideal gas law. The operating temperature and pressure are 345°C and 1 atm. However, it is not possible to find appropriate values for the effective diffusivity in Eq. (2) and the growth constants in Eq. (9). Therefore, the fitting curve based on the experiment results has been drawn.

3. Results and discussion

3.1. Comparisons of results by the crack–spallation model, the SCM, and experiments

The histories of the reaction progress, X_B, evaluated by the crack–spallation model and the SCM for the cylindrical coordinates ($N = 1$) have been plotted with respect to the reaction time with blue and red solid lines. For the comparisons, the experimental data [20] have also been plotted with the blue square marker as shown in Fig. 4.

At the beginning of the reaction, X_B is close to zero when the crack–spallation model is applied. This is due to the dominant phenomenon during this period, which is the growing of particles of U_3O_8 inside the pores. However, results by the SCM show approximately linear increasing of X_B during the same period, because the oxidation of UO_2 and the generation of an ash layer on the surface of the pellet actively occur. The experimental results show that the X_B values during the first 100 minutes are close to zero. It could be said that the better agreement with the experimental data is the result of the crack–spallation model, and not the result of the SCM. After around 150 minutes, the trend of X_B as plotted by the crack–spallation model shows a rising curve. As mentioned in the assumptions, the growth of particles is governed by the concentration of diffused O_2. Therefore, the acceleration of spallation sequence can be controlled by the diffusivity during this period. The finishing time of oxidation, which is when X_B is equal to one, can vary depending on the method of evaluation of the

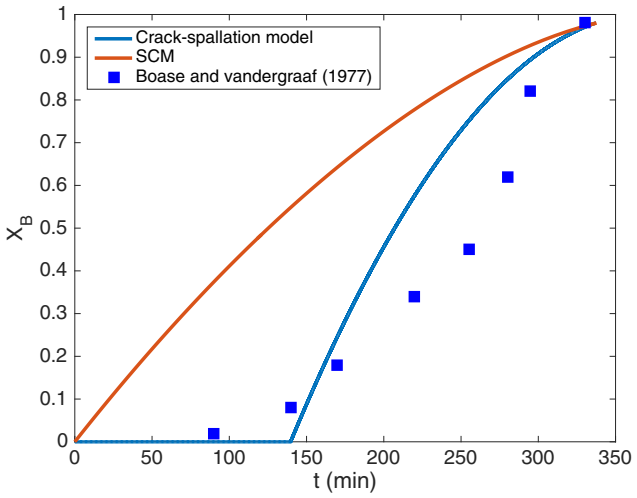

Fig. 4. Comparisons of reaction progresses among results by the crack–spallation model, the SCM, and experiments.

unknown parameters, D_e, and k for the crack–spallation model and D_e, k_{Ag}, and k_{As} for the SCM. As mentioned in the previous section, these unknown parameters are evaluated by the fitting curve approach. Better agreement with the experimental results is found in the line plotted by the crack–spallation method. Although there are some differences between results from the crack–spallation model and experiments during the middle of the entire reaction process, agreement in the major trend of the graphs can be observed. The differences could have been caused by (1) the variation of the porous type and its characteristics with respect to the radial location; (2) limited assumptions concerning the one-way radial diffusion and spallation; and (3) extra experimental conditions such as the velocity of flow.

3.2. Results depending on the geometry of the solid reactant

Results depending on different geometry for the crack–spallation model have been plotted in Fig. 5. Although the initial spallation points are very similar, rising curves after the points can be distinguished. The diffusion of O_2 converges more in the spherical

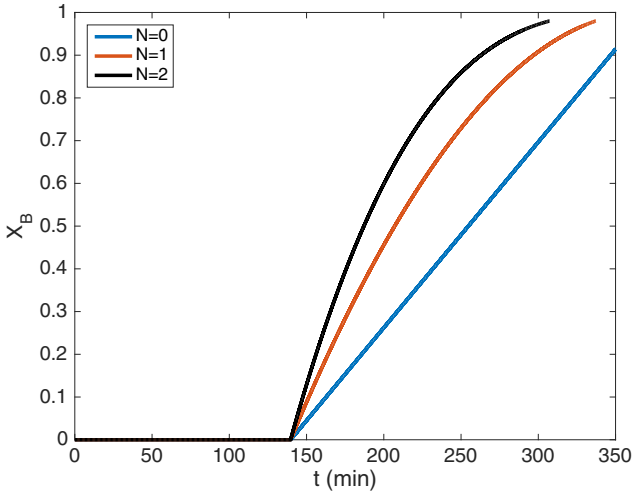

Fig. 5. Reaction progress for different geometries (N = 0: plate, N = 1: cylinder, N = 2: sphere).

case than in the cases of other geometries. Therefore, the diffusion of O_2 for the sphere geometry is the most efficient among the three geometry cases. This effect is similar to the increasing of the D_e, value as shown in the next section. Moreover, when the spallation of solid reactant occurs, the volume ratio of the spalled part to the initial solid reactant for the sphere case is greater than for the other cases, as we can see in Eq. (3).

3.3. Analysis of the crack–spallation model

Figs. 6 and 7 show temporal evolutions of the molar concentration of O_2, C_A, and the radius of U_3O_8 particles, g, in pores located at the center, the middle, and the edge of the UO_2 pellet until spallation. The line for the pore located at the center exists for the entire time domain, whereas the lines for the pores located at the middle and the edge last until their spallation points.

As we can see in Fig. 6, once O_2 diffuses into a certain location, it rapidly increases and reaches equilibrium state, which is the value of molar concentration at the outside of the pellet, C_{Ag}. Therefore, it is possible to verify the assumption for Eq. (9) that the increasing time of molar concentration is sufficiently short compared with the growth time of the product particles.

Fig. 7 shows the growth rate of product particles in pores at different locations. When the product particle size reaches the dotted line, which is the pore size used in this simulation, cracks and spallation occur. As the growth rate of the product particles is slow, a certain period is necessary to initiate cracking and spalling. At the edge of the pellet ($r = R$), the size of the product particle reaches the pore size at around 140 minutes, which is consistent with the spallation initiating point in the previous sections.

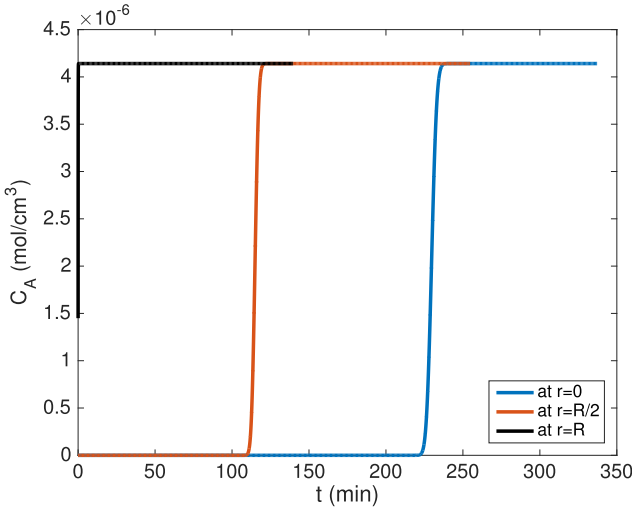

Fig. 6. Temporal evolutions of the molar concentration of O_2 in pores located at the center, middle, and edge of UO_2 pellet.

3.4. Parametric study

As mentioned in previous sections, the dominant phenomena during the crack–spallation process vary with respect to the reaction time. To understand the simulation results obtained using the crack–spallation model, a parametric study has been conducted in this section. The reference values for D_e and k have been set as 7.10×10^{-9} cm^2/s and 1.65×10^{-25} m^6/mol/s, having been determined using the fitting of the experimental results. To investigate the effects of these parameters, we define De^* and k^* as

$$D_e^* = \frac{D_e}{D_{e,ref}}, \tag{11}$$

$$k^* = \frac{k}{k_{ref}}, \tag{12}$$

where the subscript *ref* denotes a reference value.

First, the simulation results given twice and half of the reference D_e have been plotted in Fig. 8, while identical k values for three cases are used. Although different D_e values for each simulation are given, the initial spallation times are similar. The first spallation occurs at the first pores from the surface. Because the molar concentration near the surface rapidly increases and reaches a maximum point, as shown in Fig. 6, changing D_e would not significantly affect the growth rate of the product particles. However, different D_e values alter the slope of the graph. A greater value of D_e induces a faster gas diffusion into the pellet, so that the initiation of U_3O_8 particle generation deep inside the pellet occurs earlier. This triggers a faster speed of spallation.

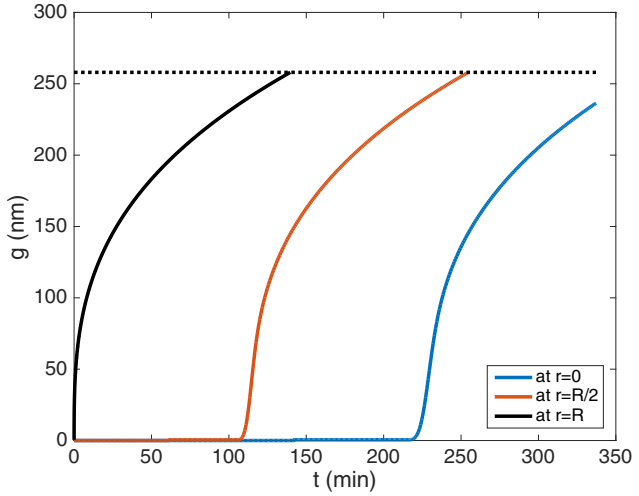

Fig. 7. Temporal evolutions of U_3O_8 particle radii in pores located at the center, middle, and edge of UO_2 pellet.

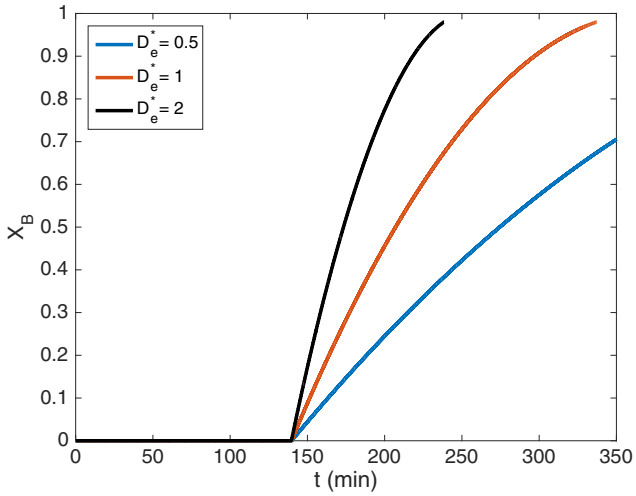

Fig. 8. Comparison of simulation results for the crack–spallation model given twice and half of the reference D_e value.

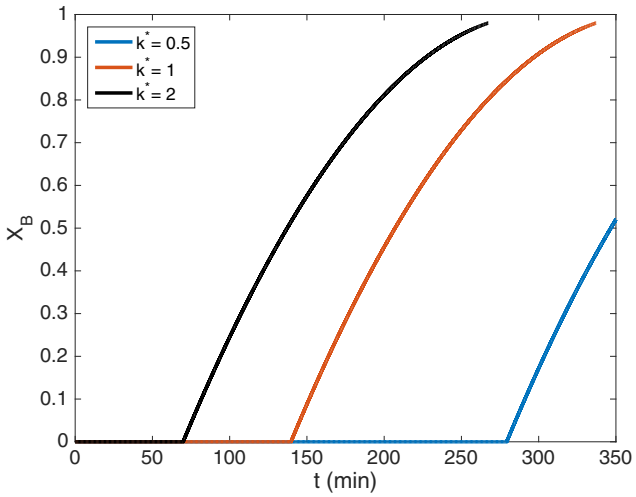

Fig. 9. Comparison of simulation results for the crack–spallation model given twice and half of the reference k value.

Second, the effect of varying k values on the simulation results has been shown in Fig. 9. The crucial change in this is the initiation times of cracks and spallation. As mentioned in the above, the first spallation occurs at the first pore layer beneath the surface. The growth of U_3O_8 particles is faster when a greater k value is given, because this value will increase the slope of the growth curve shown in Fig. 7. If the slope is steeper, the particle size reaches the pore size earlier. Therefore, the uprising points of X_B depend on the k values. However, the identical D_e values among the three cases induce similar slopes of the lines, as shown in Fig. 9. Furthermore, if the k value is much greater, the initiating time for spallation will be close to zero. Then, the trend of the result line will be in agreement with the line from the SCM.

4. Conclusion

The crack–spallation model has been newly developed to analyze gas–solid reactions dominated by the order of diffusing of the gas reactant into the solid reactant, the growth of product particles in the pores, and the cracks and spallation of the solid reactant. The governing equations for this new method mainly consist of two parts: (1) a partial differential equation for the diffusion process and (2) an ordinary differential equation representing the growth of product particles. These equations can be solved by numerical and analytical approaches. To mimic the spallation process, new boundary conditions are applied to the diffusion equation when the particle size is larger than the size of the pore.

This model has been validated using the oxidation process of UO_2. Because of a lack of information needed to model the experiment circumstance, several assumptions for the size of pores and the molar concentration of gas have been made, and a fitting method for D_e and k has been appropriately applied. In addition, to support a robust discussion of this method, a well-known method for gas–solid reactions, the SCM, has been compared. The results of this validation can be summarized as showing that the crack–spallation model yields better agreement with the experimental data than does the SCM. Because the crack–spallation model includes the process of product particle growth inside of the solid reactant, it can precisely represent the trigger time of the reaction progress.

Moreover, a parametric study of the dominant parameters, D_e and k, has been conducted. For that, the parameter values were intentionally varied to twice and half of the fitted reference values. The results of the parametric study clearly show how the D_e and k parameters change the reaction progress as a function of time. D_e is able to vary the slope of the reaction progress, whereas the initiating time for cracks and spallation of the solid reactant relies on the k parameter.

Although the results of the crack–spallation model are not exactly consistent with those from the experiments, this new method can reasonably and effectively illustrate the process of gas–solid reactions dominated by the growth of product in each pore and spallation of the solid reactant. This model can be improved by applying more practical modeling and by adding parameters.

Conflict of interest

There is no conflict of interests.

References

[1] S. Yagi, D. Kunii, Studies on combustion of carbon particles in flames and fluidized beds, Symp. (Int.) Combust. 5 (1) (1955) 231–244, https://doi.org/10.1016/S0082-0784(55)80033-1.
[2] O. Levenspiel, Chemical Reaction Engineering, John Wiley & Sons, New York, 1999.
[3] R.W. Missen, C.A. Mims, B.A. Saville, Introduction to Chemical Reaction Engineering and Kinetics, John Wiley & Sons, New York, 1999.
[4] S.M. Jeong, J.-M. Hur, H. Lee, Kinetic modelings study of a voloxidation for the production of U_3O_8 powder from a UO_2 pellet, Nucl. Eng. Technol. 41 (8) (2009) 1073–1078, https://doi.org/10.5516/NET.2009.41.8.1073.
[5] P.K. Gbor, C.Q. Jia, Critical evaluation of coupling particle size distribution with the shrinking core model, Chem. Eng. Sci. 59 (10) (2004) 1979–1987, https://doi.org/10.1016/j.ces.2004.01.047.
[6] S. Homma, S. Ogata, J. Koga, S. Matsumoto, Gas–solid reaction model for a shrinking spherical particle with unreacted shrinking core, Chem. Eng. Sci. 60 (18) (2005) 4971–4980, https://doi.org/10.1016/j.ces.2005.03.057.
[7] B.H. Shi, S.S. Fan, X. Lou, Application of the shrinking-core model to the kinetics of repeated formation of methane hydrates in a system of mixed dry-water and porous hydrogel particulates, Chem. Eng. Sci. 109 (2014) 315–325, https://doi.org/10.1016/j.ces.2014.01.035.
[8] Z. Xu, X. Sun, M.A. Khaleel, A generalized kinetic model for heterogeneous gas-solid reactions, J. Chem. Phys. 137 (7) (2012), https://doi.org/10.1063/1.4740242, 074702–074702.
[9] K.K. Bae, B.G. Kim, Y.W. Lee, M.S. Yang, H.S. Park, Oxidation behavior of unirradiated UO_2 pellets, J. Nucl. Mater. 209 (3) (1994) 274–279, https://doi.org/10.1016/0022-3115(94)90263-1.
[10] W.I. Ko, H.H. Lee, S. Choi, S.K. Kim, B.H. Park, H.J. Lee, I.T. Kim, H.S. Lee, Preliminary conceptual design and cost estimation for Korea Advanced Pyroprocessing Facility Plus (KAPF+), Nucl. Eng. Des. 277 (2014) 212–224, https://doi.org/10.1016/j.nucengdes.2014.06.033.
[11] J.H. Goode, Voloxidation – Removal of Volatile Fission Products from Spent LMFBR Fuels, Tech. rep., Oak Ridge National Laboratory, 1973.
[12] S.K. Kim, W.I. Ko, S.R. Youn, R. Gao, Cost analysis of a commercial pyroprocess facility on the basis of a conceptual design in Korea, Ann. Nucl. Energy 80 (2015) 28–39, https://doi.org/10.1016/j.anucene.2015.01.011.
[13] B.H. Park, C.-S. Seo, A semi-empirical model for the air oxidation kinetics of UO_2, Korean J. Chem. Eng. 25 (1) (2008) 59–63, https://doi.org/10.1007/s11814-008-0010-9.
[14] K.C. Song, G. Park, J.W. Lee, J.J. Park, Fractional release behavior of volatile and semivolatile fission products during a voloxidation and OREOX treatment of spent PWR fuel, Nucl. Technol. 162 (May) (2008) 158–168.
[15] J.-H. Yoo, C.-S. Seo, E.-H. Kim, H.-S. Lee, A conceptual study of pyroprocessing for recovering actinides from spent oxide fuels, Nucl. Eng. Technol. 40 (7) (2008) 581–592, https://doi.org/10.5516/NET.2008.40.7.581.
[16] F. Gao, W.I. Ko, C.J. Park, S.K. Kim, H.H. Lee, Modeling and criticality evaluation of the voloxidation process, Ann. Nucl. Energy 38 (10) (2011) 2187–2194, https://doi.org/10.1016/j.anucene.2011.06.014.
[17] C.J. Park, J.J. Park, K.C. Song, Shielding analysis for an advanced voloxidation process with Monte Carlo calculations, Ann. Nucl. Energy 36 (5) (2009) 694–699, https://doi.org/10.1016/j.anucene.2009.01.003.
[18] J.A. Johnson, Studies of Reaction Processes for Voloxidation Methods, Ph.D. thesis, University of Tennessee, Knoxville, 2013.
[19] S. Kashibe, K. Une, K. Nogita, Formation and growth of intragranular fission gas bubbles in UO_2 fuels with burnup of 6-83 GWd/t, J. Nucl. Mater. 206 (1993) 22–34, https://doi.org/10.1016/0022-3115(93)90229-R.
[20] D.G. Boase, T.T. Vandergraaf, The Canadian spent fuel storage canister: some materials aspects, Nucl. Technol 32 (1977) 60–71.